



## RESEARCH LETTER

10.1002/2015GL065245

## Key Points:

- EMIC waves and MeV electron precipitation are observed at the same UT and MLT
- EMIC wave and precipitation timing, extent, and drivers are examined
- Results provide observational confirmation of duskside EMIC-electron interactions

## Correspondence to:

L. W. Blum,  
lwblum@ssl.berkeley.edu

## Citation:

Blum, L. W., et al. (2015), Observations of coincident EMIC wave activity and duskside energetic electron precipitation on 18–19 January 2013, *Geophys. Res. Lett.*, 42, 5727–5735, doi:10.1002/2015GL065245.

Received 6 JUL 2015

Accepted 10 JUL 2015

Accepted article online 14 JUL 2015

Published online 30 JUL 2015

## Observations of coincident EMIC wave activity and duskside energetic electron precipitation on 18–19 January 2013

L. W. Blum<sup>1</sup>, A. Halford<sup>2</sup>, R. Millan<sup>2</sup>, J. W. Bonnell<sup>1</sup>, J. Goldstein<sup>3</sup>, M. Usanova<sup>4</sup>, M. Engebretson<sup>5</sup>, M. Ohnsted<sup>5</sup>, G. Reeves<sup>6</sup>, H. Singer<sup>7</sup>, M. Clilverd<sup>8</sup>, and X. Li<sup>4</sup>

<sup>1</sup>Space Sciences Laboratory, University of California, Berkeley, California, USA, <sup>2</sup>Department of Physics and Astronomy, Dartmouth College, Hanover, New Hampshire, USA, <sup>3</sup>Southwest Research Institute, San Antonio, Texas, USA, <sup>4</sup>Laboratory for Atmospheric and Space Physics, Boulder, Colorado, USA, <sup>5</sup>Department of Physics, Augsburg College, Minneapolis, Minnesota, USA, <sup>6</sup>Los Alamos National Laboratory, Los Alamos, New Mexico, USA, <sup>7</sup>NOAA Space Weather Prediction Center, Boulder, Colorado, USA, <sup>8</sup>British Antarctic Survey, Cambridge, UK

**Abstract** Electromagnetic ion cyclotron (EMIC) waves have been suggested to be a cause of radiation belt electron loss to the atmosphere. Here simultaneous, magnetically conjugate measurements are presented of EMIC wave activity, measured at geosynchronous orbit and on the ground, and energetic electron precipitation, seen by the Balloon Array for Radiation belt Relativistic Electron Losses (BARREL) campaign, on two consecutive days in January 2013. Multiple bursts of precipitation were observed on the duskside of the magnetosphere at the end of 18 January and again late on 19 January, concurrent with particle injections, substorm activity, and enhanced magnetospheric convection. The structure, timing, and spatial extent of the waves are compared to those of the precipitation during both days to determine when and where EMIC waves cause radiation belt electron precipitation. The conjugate measurements presented here provide observational support of the theoretical picture of duskside interaction of EMIC waves and MeV electrons leading to radiation belt loss.

### 1. Introduction

Wave-particle interactions play a critical role in radiation belt dynamics, providing a source of both acceleration and loss of energetic electrons in the inner magnetosphere. Particle precipitation into the atmosphere due to pitch angle scattering by waves is an important loss process, the causes and consequences of which are of great interest to the radiation belt community. Among these waves are electromagnetic ion cyclotron (EMIC) waves, which can resonate with MeV electrons and scatter them into the loss cone (see *Millan and Thorne* [2007] for a review). EMIC waves are generated by anisotropic ion distributions and are often observed on the duskside of the inner magnetosphere, where freshly injected ions drift in from the tail [*Cornwall et al.*, 1970; *Anderson et al.*, 1996]. They have also been observed in the morning sector and across the dayside at larger radial distances during compressions of the dayside magnetosphere [e.g., *Anderson and Hamilton*, 1993; *Keika et al.*, 2013]. Duskside EMIC waves occur more often in the helium ( $\text{He}^+$ ) band (between the oxygen and helium cyclotron frequencies) and with left-hand polarization, while the dawnside and dayside EMIC waves tend to lie in the hydrogen ( $\text{H}^+$ ) band (between the helium and hydrogen cyclotron frequencies) and are more often linearly or right-hand polarized [*Min et al.*, 2012]. Wave occurrence rates in both regions peak during geomagnetic storms and substorms as well as periods of enhanced solar wind dynamic pressure [*Erlanson and Ukhorskiy*, 2001; *Halford et al.*, 2010; *Usanova et al.*, 2012]. Theory and simulations have shown that strong resonant interactions can occur between EMIC waves and MeV electrons, leading to the hypothesis that these waves are a source of precipitation and loss of radiation belt electrons [*Lyons and Thorne*, 1972; *Summers and Thorne*, 2003; *Ukhorskiy et al.*, 2010]. The presence of dense cold plasma lowers the minimum resonant energy of radiation belt electrons interacting with EMIC waves; thus, the duskside of the magnetosphere, where cold, dense plasmaspheric bulges and plumes extend and overlap ring current ions, has been suggested as a preferential region for EMIC-electron interactions [e.g., *Thorne and Kennel*, 1971; *Jordanova et al.*, 2008].

MeV electron precipitation has been observed by a number of different platforms, including balloons and low-altitude satellites. While millisecond-long microburst precipitation occurs primarily on the dawnside of the magnetosphere, measurements of longer-duration MeV electron precipitation all show a peak in

occurrence in the dusk sector [Nakamura *et al.*, 2000; Carson *et al.*, 2013; Comess *et al.*, 2013; Wang *et al.*, 2014; Blum *et al.*, 2015]. During the MeV Auroral X-ray Imaging and Spectroscopy (MAXIS) balloon campaign, electron precipitation was observed at all local times in the magnetosphere, but the harder-spectrum relativistic electron precipitation, or “REP”, events were constrained to the duskside, between noon and midnight [Millan *et al.*, 2002]. Radial and local time distributions of MeV precipitation events have led many to suggest that they are the observational signatures of EMIC wave interaction with and scattering of radiation belt electrons [Vampola, 1977; Bortnik *et al.*, 2006]. Imhof *et al.* [1986] found simultaneous keV ion and MeV electron precipitation on a number of occasions, a signature often associated with EMIC wave scattering as these waves can resonate with both these particle populations [e.g., Sandanger *et al.*, 2007]. Such concurrent ion and electron precipitation was observed along with ground-based measurements of EMIC waves by Miyoshi *et al.* [2008] on 5 September 2005. During another event on 17 January 2013, Li *et al.* [2014] modeled the expected radiation belt electron precipitation spectrum from an observed EMIC wave event and found good agreement with balloon-measured precipitation.

Here we present further observational evidence for the association between duskside relativistic electron precipitation and EMIC waves via magnetically conjugate measurements from the Balloon Array for Radiation belt Relativistic Electron Losses (BARREL) balloon 1C and GOES 13. Two periods of relativistic electron precipitation and EMIC wave activity are observed on two consecutive days in January 2013. The solar wind and geomagnetic conditions during these events are investigated to reveal the temporal and spatial characteristics of the observed waves and precipitation as well as the conditions under which these events can occur.

## 2. Primary Observations

Two BARREL balloon campaigns were conducted out of Antarctica during January–February 2013 and 2014. A summary of the mission and balloon instrumentation can be found in Millan *et al.* [2013]. On any given day during the campaigns, multiple balloons were aloft at a range of local times and latitudes, providing an array of measurements spanning the foot points of the outer radiation belt [Woodger *et al.*, 2015]. At their altitude of ~30 km, the balloons measure bremsstrahlung X-rays produced by precipitating electrons impacting Earth’s atmosphere, rather than the precipitating electrons directly.

Figure 1a shows the X-ray spectrogram measured by BARREL balloon 1C on 18–19 January 2013. Three large bursts of precipitation occurred from 22:00 UT 18 January to 01:00 UT 19 January, followed by four more bursts roughly 24 h later, at the end of 19 January (precipitation periods are marked by dashed purple lines in Figure 1). Each of these precipitation events produced X-rays of energies exceeding ~500 keV at count rates above background levels, indicating that relativistic electron precipitation was occurring. Precipitating 0.5–1.6 and 1.6–3.8 MeV electrons were also observed at a magnetically conjugate location by the Colorado Student Space Weather Experiment (CSSWE), a CubeSat in low-Earth orbit [Li *et al.*, 2012], during the first set of precipitation bursts. (CSSWE was not in the right location to observe the second set, see Blum *et al.* [2013] for further details.) Figure 1b shows the magnetic spectral density measured by the GOES 13 magnetometer, with 0.512 s sampling period, during the same 2 day period. Local  $O^+$ ,  $He^+$ , and  $H^+$  ion gyrofrequencies are indicated by the white lines. EMIC wave activity was observed in the  $H^+$  band from ~12:00 UT 18 January to ~01:00 UT 19 January. This subsided until later on 19 January when bursts of wave activity were observed first in the  $H^+$  band ~18:00 UT and later in the  $H^+$  and  $He^+$  bands at ~21:30–23:30 UT. Some  $O^+$  band wave activity may also have been present but is difficult to distinguish from other more broadband signatures during this period.

Figures 1c–1g present solar wind conditions and geomagnetic indices for the same 2 day period in January 2013. Interplanetary magnetic field (IMF)  $B_z$ , solar wind dynamic pressure  $P_{dyn}$ , and interplanetary electric field (IEF)  $E_y$ , a measure of magnetospheric convection, are displayed in Figures 1c, 1d, and 1e, respectively. These are provided by the OMNI database and have been time shifted to the nose of Earth’s bow shock. Below these, in Figures 1f and 1g, are  $AE$  and  $SYM-H$  indices, also from the OMNI database. Two pressure pulses occurred under northward IMF, marked by the red vertical dashed lines around 12:00 UT 18 January and 18:00 UT 19 January, both of which were accompanied by EMIC wave activity observed by GOES 13. Some time after each of these pulses,  $B_z$  turned southward, IEF  $E_y$  became positive, and substorm activity commenced. During these periods, electron precipitation and strong EMIC wave activity were

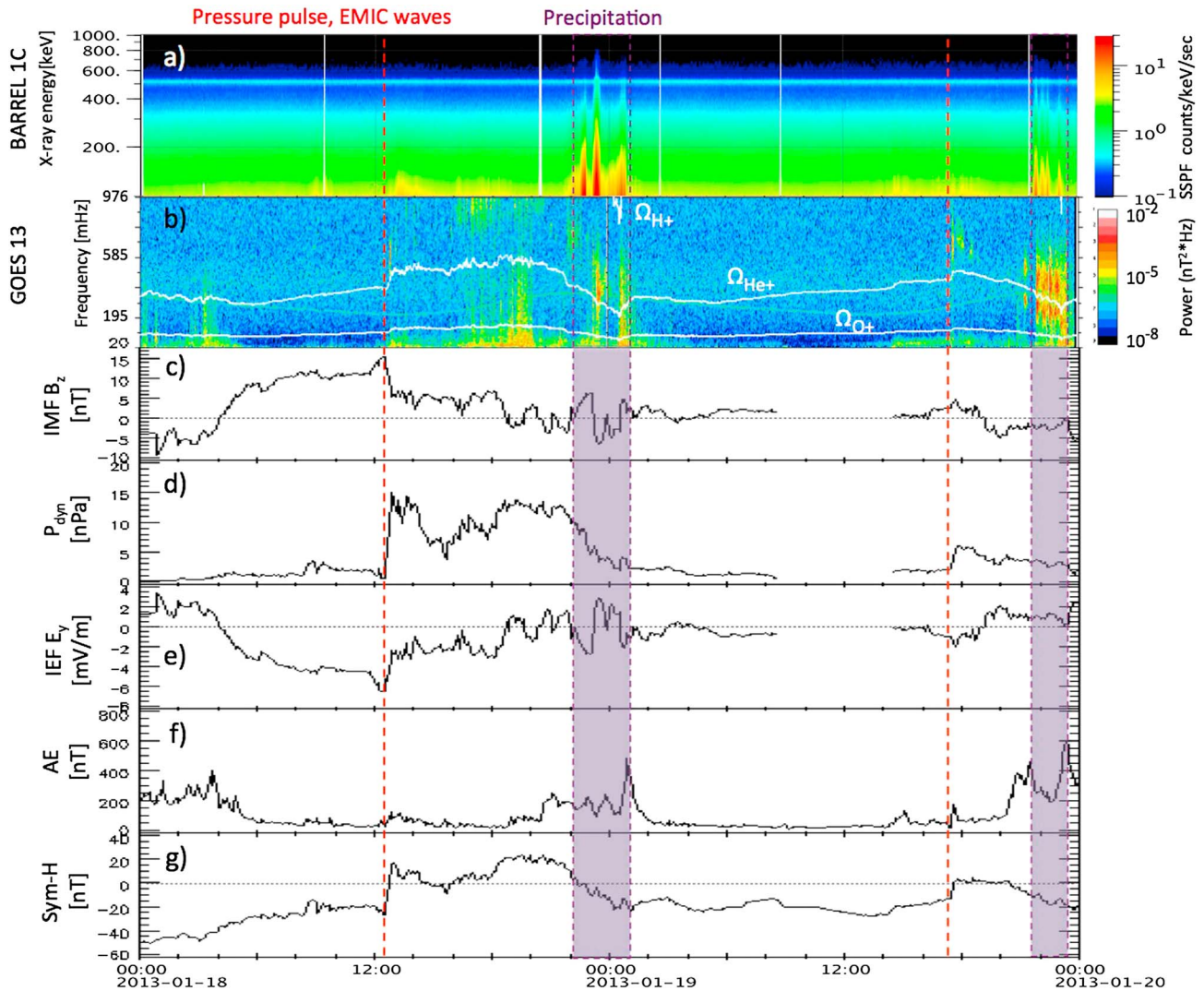


**Figure 1.** (a) BARREL balloon 1C observations, (b) GOES 13 wave measurements, (c–e) solar wind conditions, and (f and g) geomagnetic AE and SYM-H indices on 18–19 January 2013. The red vertical dashed lines mark the sudden enhancements in the solar wind dynamic pressure and the purple dashed lines and shaded regions the times of relativistic electron precipitation.

observed, marked by the purple dashed lines and shaded regions. Following the recovery phase of a geomagnetic storm on 17 January 2013, the SYM-H index remained above  $\sim -25$  nT during these periods (see Figure 1g), indicating a very weak geomagnetic storm signature, if any at all.

Figure 2 shows the location, in  $L$  shell and magnetic local time (MLT), of the equatorial foot points of balloon 1C and GOES 13 during the two precipitation periods. Figure 2a is a snapshot of the inner magnetosphere at 23:00 UT 18 January, during the first set of precipitation bursts, and Figure 2b from 22:00 UT 19 January, at the start of the second period of precipitation. In each panel, locations of the six Los Alamos National Laboratory (LANL) geosynchronous satellites, whose observations will be discussed in the following section, are marked with colored circles, GOES 13 and GOES 15 with dark and light pink triangles, and balloon 1C with a purple square. The purple lines indicate the trajectory of balloon 1C over the few-hour periods of precipitation. The balloon location and path have been mapped to the equatorial plane using the T89 magnetic field model, with  $Kp$  as an input [Tsyganenko, 1989], which has been shown to accurately map on the duskside during periods of quiet to moderate geomagnetic activity such as the ones presented here [McCollough et al., 2008]. Throughout the 2 day period, balloon 1C and GOES 13 remained roughly aligned in MLT and within  $\sim 1.5L$  shells of each other. An additional BARREL balloon, 1G, tracked closely in MLT to balloon 1C and mapped to  $L = 7-8$  on the dayside (and  $L > 8$  on the duskside) during this period. This balloon did not

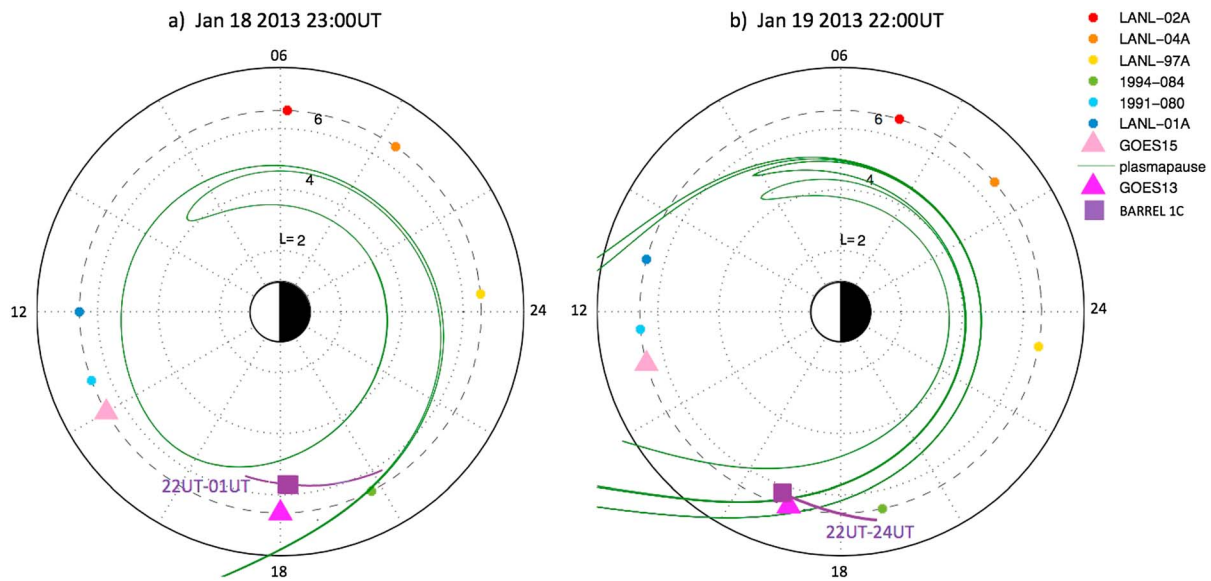


**Figure 2.** (a and b) Snapshots of the inner magnetosphere during the two precipitation periods. GOES spacecraft are marked with triangles; LANL geosynchronous satellites with circles; the mapped location of balloon 1C with a square; and the plasmopause, as calculated by test-particle simulations [Goldstein *et al.*, 2014a], in dark green. The balloon trajectory during the duration of the precipitation events, calculated using T89, is shown with the solid purple line. Local noon is to the left.

see any radiation belt precipitation during this 2 day period, consistent with balloon 1C's dayside observations. The location of the plasmopause, as determined from test particle simulations described in Goldstein *et al.* [2014a] and driven by  $K_p$  and IEF  $E_y$ , is shown in dark green. Extended density structures and remnant plasmaspheric plumes wrapped around the night and afternoon sectors appear on both occasions.

Figures 1 and 2 show the close alignment in space and time of radiation belt electron precipitation measured by BARREL balloon 1C and EMIC wave activity observed by GOES 13. Figure 2 also shows that the location of balloon 1C during these events mapped to a region near dusk likely to contain dense plasmaspheric plume material and structure. The next section presents additional wave and particle measurements to investigate further the timing and distribution of the waves, as well as the associated geomagnetic conditions during the two precipitation events.

### 3. Discussion: EMIC Wave Timing, Extent, and Drivers

In addition to the EMIC wave observations at GOES 13, spectrograms from GOES 15 and ground stations at Halley and the Canadian Array for Real-time Investigations of Magnetic Activity (CARISMA) network are shown in Figure 3. The Halley and GOES spectrograms were produced by applying a 256-point fast Fourier transform (FFT) to differenced magnetic field data. The GOES data [Singer *et al.*, 1996] were sampled at 0.512 s cadence (~2 Hz sampling rate), and Halley data [Engebretson *et al.*, 2008] were originally sampled at 10 Hz but averaged to 2 Hz for this study. CARISMA spectrograms were generated using a sliding window FFT applied to induction coil magnetometer data ( $\leq 0.2$  pT/Hz sensitivity at 1 Hz, 30 Hz Nyquist frequency) [Mann *et al.*, 2008]. The times of the pressure pulses, identified in Figure 1, are marked here as well by the vertical dashed red lines. The solar wind dynamic pressure enhancements around 12:00 UT 18 January and 18:00 UT 19 January generate waves across the dayside magnetosphere, measured by GOES 13 and multiple ground stations, including Halley, FCHU, and DAWs. Compressions of the magnetopause are able to generate anisotropic ion populations, the free energy source for EMIC wave growth, across the dayside magnetosphere due to drift shell splitting, Shabansky orbits, and adiabatic heating [Olson and Lee, 1983; McCollough *et al.*, 2010]. Observations have shown that EMIC wave occurrence rates increase across the dayside magnetosphere, particularly at larger radial distances ( $L > 6$ ), during periods of enhanced solar wind dynamic pressure [Anderson and Hamilton, 1993; Usanova *et al.*, 2012]. These dayside EMIC waves often occur in the  $H^+$  band, consistent with the wave observations on these 2 days, while EMIC waves observed on the duskside at and within geosynchronous orbit are more often of larger amplitude and at lower frequencies, below the  $He^+$  gyrofrequency [Min *et al.*, 2012; Keika *et al.*, 2013; Meredith *et al.*, 2014],

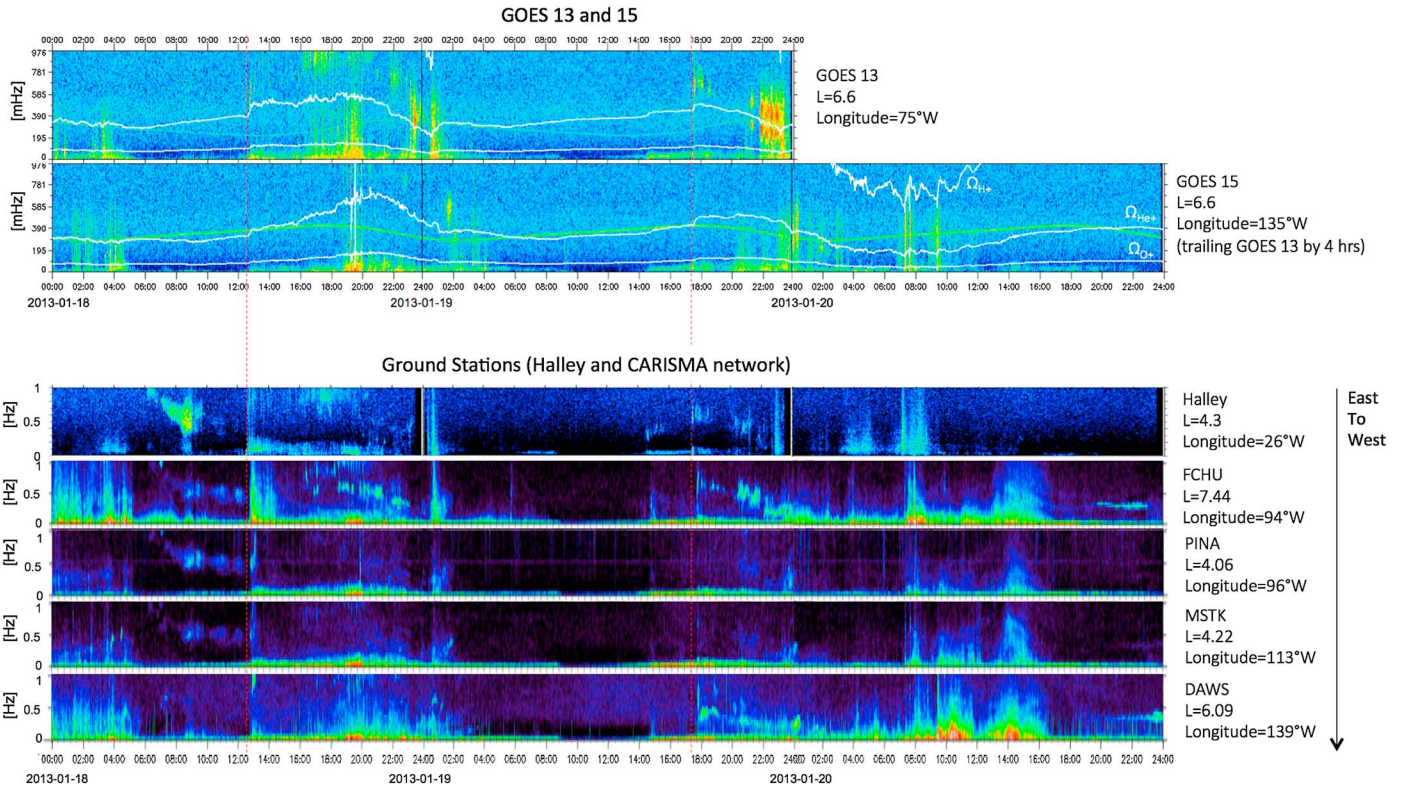


**Figure 3.** (top) GOES 13 and GOES 15 spectrograms and (bottom) ground observations from Halley and the CARISMA network on 18–20 January 2013. GOES 15 trails GOES 13 by 4 h, and the CARISMA ground stations span longitudes roughly between the two GOES satellites. The red vertical dashed lines mark the times of sudden increases in the solar wind dynamic pressure, as identified in Figure 1.

as was seen during the precipitation event late on 19 January. Conversely, the precipitation event on 18 January appears in association with  $H^+$  band waves. However, balloon 1C maps further inside geosynchronous orbit, and closer to the model plasmopause, during this period (see Figure 2), and there is a less direct correlation between the bursty precipitation and wave structure than was seen at the end of 19 January; thus, it is possible that the waves generating the precipitation observed at balloon 1C have different characteristics than those measured by GOES during this first event. Simulations by Denton *et al.* [2014] suggest that  $He^+$  band EMIC wave excitation is preferred in high-density plasma, while  $H^+$  band waves are more likely to occur in the plasma trough. This would be consistent with the location of balloon 1C at the plasmopause, measuring precipitation driven by  $He^+$  EMIC waves, while GOES 13 was further out in the plasma trough and measured  $H^+$  band waves (Figure 2a). The particular frequency band of EMIC waves can influence the range of electron energies precipitated, particularly the lower cutoff energy [e.g., Clilverd *et al.*, 2015], and in the cold plasma approximation, waves below and approaching the  $He^+$  gyrofrequency can resonate most easily with radiation belt electrons of lower energy [e.g., Ukhorskiy *et al.*, 2010].

In addition to these wave observations, particle measurements from geosynchronous orbit also exist from this period. LANL Synchronous Orbit Particle Analyzer (SOPA) measurements of energetic ions and electrons are available from six geosynchronous satellites, distributed in MLT as shown in Figure 2. Figure 4 shows six electron (Figure 4a) and ion (Figure 4b) energy channels, ranging from 50 keV to ~1 MeV, from each spacecraft. Particle injections can be seen in both species, at multiple spacecraft, from just before 21:00 UT on 18 January to ~03:00 UT 19 January (left) and again around 20:00–24:00 UT on 19 January (right). The relative dispersion of these injections measured at different spacecraft, at different local times, suggests that the particles were injected in the midnight sector, with electrons drifting around to the dawn and ions to the dusk. Dawnward propagation of electrons can be observed, for example, around 23:00 UT 19 January, when a dispersionless injection appeared first at LANL-97A (close to midnight MLT), becoming more dispersed in energy as it reached LANL-04A, 02A, 01A, etc. (downward through the panels of Figure 4). The reverse pattern is observed in the ions at this time, the injection starting at 1994–084 and becoming more dispersed moving

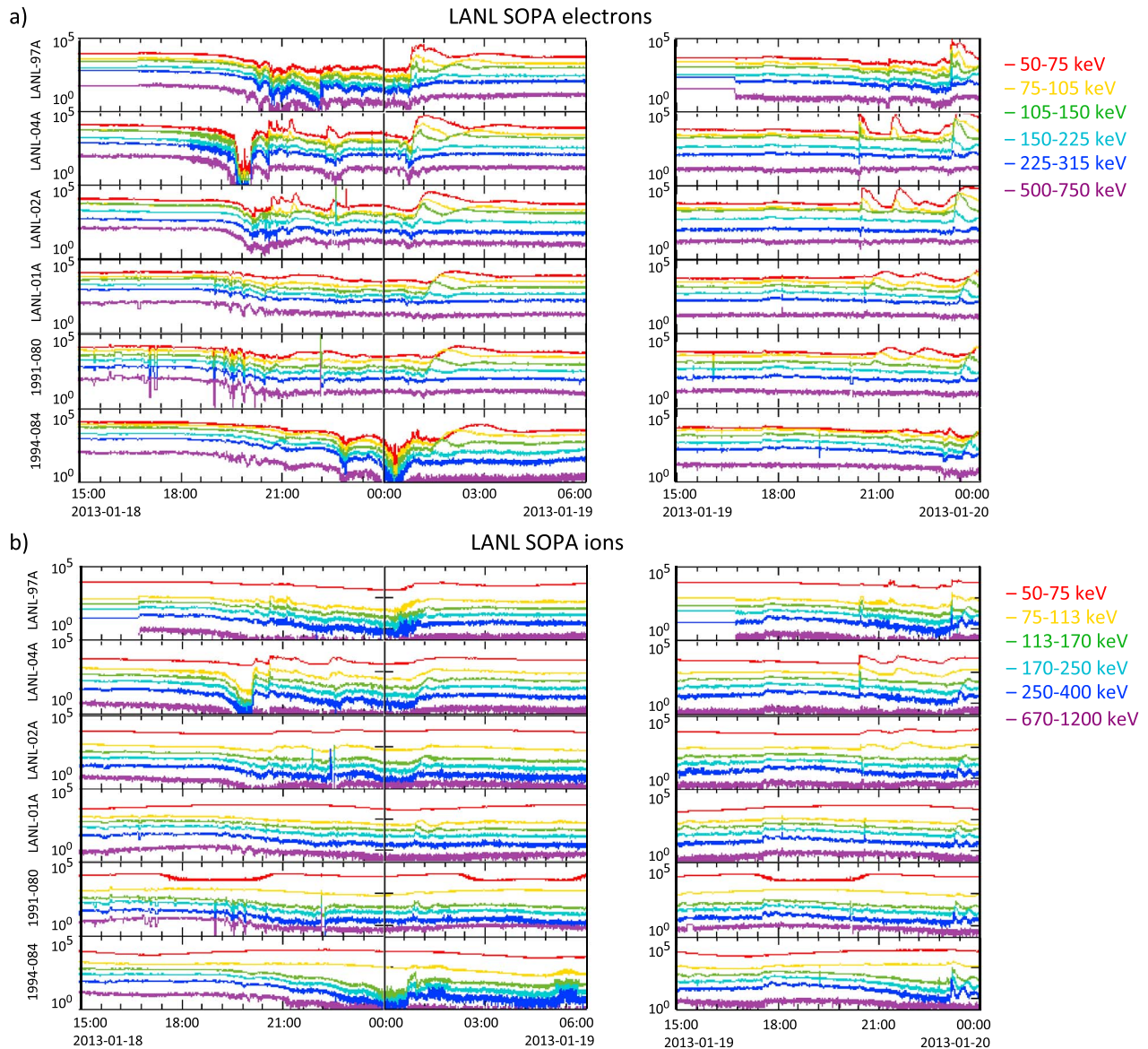


**Figure 4.** LANL SOPA electron and ion observations (50 keV to ~1 MeV) from six geosynchronous spacecraft distributed in local time. Injection signatures, both dispersed and dispersionless, are visible in the ions and electrons (left) from ~21:00 UT 18 January to 02:00 UT 19 January and (right) again at ~20:00–24:00 UT 19 January. Note that the lower energy proton channels have high background noise levels that mask some of the dynamics at those energies.

up through the panels of Figure 4. In addition to magnetopause compressions, particle injections can provide a free energy source for EMIC wave growth as well, bringing fresh anisotropic ion populations to the duskside through adiabatic heating [Cornwall and Schulz, 1971; Jordanova et al., 2006]. Lorentzen et al. [2000] observed similar particle injections during an MeV electron precipitation event measured by a balloon as part of the 1996 Interball and Balloon Observations of Aurora (INTERBOA) campaign [Foat et al., 1998], but they did not have any direct wave observations with which to compare.

While anisotropic ion distributions provide the free energy source for EMIC waves, cold plasma can play a role both in EMIC wave growth as well as resonant interactions with radiation belt electrons [e.g., Thorne and Kennel, 1971; Gendrin, 1975]. Figure 2 shows that balloon 1C and GOES 13 lie just outside the model plasmopause during the precipitation events, between this boundary and remnant plume structures. During this period, the test particle-modeled plasmopause crossings were within ~0.4  $R_E$  of measured crossings by the Van Allen Probes, whose apogee was in the postmidnight sector [Goldstein et al., 2014a].

The long-lived remnant plume structures that frequently appear in the simulations have also been observed by spacecraft, but there is often a significant amount of density structure measured within these features that is not captured by the simulations [Goldstein *et al.*, 2014b]. While the exact location of the remnant plumes and plasmopause shown in Figure 2 may not be accurate, the simulation results suggest that there were likely substantial density enhancements and structure in the area around balloon 1C and GOES 13 during the precipitation events, particularly during the second precipitation event late on 19 January. During the first precipitation event, balloon 1C lies close to the plasmopause, while GOES 13 may lie in the plasma trough, as was discussed earlier and which would be consistent with the observed EMIC wave frequency spectrum. Simulations have shown that, in addition to enhanced cold plasma density, density gradients can be associated with EMIC wave growth as well [Chen *et al.*, 2009; de Soria-Santacruz *et al.*, 2013]; however, observational evidence of this is still lacking [e.g., Halford *et al.*, 2015]. Thus, this cold plasma density structure may play a range of roles in the EMIC wave growth and electron precipitation observed on the duskside during these events. However, the lack of direct density measurements in these events precludes a more detailed study of those effects here.

The 2 day period examined here exhibited solar wind pressure enhancements coincident with EMIC waves observed across the dayside magnetosphere. However, it was not until a few hours after each pressure pulse, during enhanced magnetospheric convection, substorm activity, and particle injections, as balloon 1C and GOES 13 came into the dusk sector, that MeV electron precipitation was observed in close conjunction with the EMIC waves. The injection signatures and multipoint wave observations, combined with the solar wind conditions shown in Figure 1, suggest that there were two separate precipitation events occurring in a similar region on two consecutive days, rather than the same event persisting as GOES 13 and balloon 1C drifted back around to the duskside. These observations demonstrate the importance of wave properties and drivers and ambient plasma conditions for determining when EMIC waves may cause relativistic electron precipitation. In the events shown here, it is the duskside EMIC waves observed during periods of enhanced convection and substorm activity that are effective at driving radiation belt loss, rather than the dayside H<sup>+</sup> band EMIC waves generated by compressions of the magnetopause. The combination of larger wave amplitude, wave frequencies closer to the He<sup>+</sup> gyrofrequency, and enhanced cold plasma density and structure on the duskside may all contribute to a lower minimum electron resonant energy and stronger scattering rates, thus leading to efficient radiation belt electron precipitation. The relative contribution of injections as compared to concurrent enhanced global convection and the reconfiguration of the plasmasphere for EMIC wave generation and resonance with MeV electrons will be explored in future investigations. The examples shown here provide a possible explanation for differences in the global distributions of EMIC waves, often observed across the day and afternoon sectors, and MeV electron precipitation events, whose occurrence rates peak between dusk and midnight. Determining when and where EMIC waves resonate with and scatter radiation belt electrons has important implications for assessing the loss rate due to these waves.

#### 4. Summary

Simultaneous, magnetically conjugate measurements of energetic electron precipitation, as observed by BARREL, and EMIC wave activity, seen by GOES 13, are presented from a period in January 2013. Two periods of precipitation were observed on consecutive days, each occurring during periods of enhanced convection, energetic particle injections, and substorm activity. Both events occurred as balloon 1C drifted across the dusk sector at latitudes mapping to the outer radiation belt close to geosynchronous orbit, during which times GOES 13 observed strong EMIC wave activity with similar structure and modulation as the observed precipitation. This work presents an important first step toward determining when and where EMIC waves resonate with and scatter MeV electrons and why the dusk sector is the favorable region for precipitation loss of radiation belt electrons. A summary of the observations as well as their implications are given below:

1. Concurrent wave and precipitation measurements provide strong observational support of the theoretical picture of duskside interaction between EMIC waves and MeV electrons leading to precipitation.
2. EMIC wave activity and radiation belt precipitation losses occurred during this period under substorm activity alone, without an associated geomagnetic storm.

3. Solar wind pressure pulses generated EMIC waves across the dayside magnetosphere, but it was the duskside wave activity, associated with nightside particle injections and enhanced magnetospheric convection, that was observed to be radiation belt effective during these events on 18–19 January 2013.

#### Acknowledgments

This work was supported in part by the JHU/APL contract 922613 (RBSP-EFW). The Dartmouth portion of this work was supported by the BARREL grant NNX08AM58G. X. Li acknowledges NASA grant NNX15AF56G. Work at Augsburg College and provision of search coil data from Halley, Antarctica, were supported by NSF grant PLR-1341493. Test particle simulations (JG) were supported by the NASA Van Allen Probes mission's RBSP-ECT project. M.A.C. has received funding from the Natural Environmental Research Council under the Antarctic Funding Initiative (AFI/11/22). This work was also supported by the International Space Science Institute International Teams program. The authors thank I.R. Mann, D.K. Milling, and the rest of the CARISMA team for data, which can be accessed at [www.carisma.ca](http://www.carisma.ca). CARISMA is operated by the University of Alberta and funded by the Canadian Space Agency. Halley spectrograms can be accessed at [space.augsburg.edu/searchcoil/browsehalley-graphs.html](http://space.augsburg.edu/searchcoil/browsehalley-graphs.html). The OMNI data were obtained from the GSFC/SPDF OMNIWeb interface at <http://omniweb.gsfc.nasa.gov>, which are derived from ACE and Wind solar wind plasma and magnetic field observations. BARREL measurements can be found at <http://cdaweb.gsfc.nasa.gov/> and GOES at <http://satdat.ngdc.noaa.gov/sem/goes/>. LANL SOPA data were provided by G. Reeves ([reeves@lanl.gov](mailto:reeves@lanl.gov)) and are available upon request.

The Editor thanks two anonymous reviewers for their assistance in evaluating this paper.

#### References

- Anderson, B. J., and D. C. Hamilton (1993), Electromagnetic ion cyclotron waves stimulated by modest magnetospheric compressions, *J. Geophys. Res.*, *98*, 11,369–11,382, doi:10.1029/93JA00605.
- Anderson, B. J., R. E. Denton, G. Ho, D. C. Hamilton, S. A. Fuselier, and F. J. Strangeway (1996), Observational test of local proton cyclotron instability in the Earth's magnetosphere, *J. Geophys. Res.*, *101*, 21,527–21,543, doi:10.1029/96JA01251.
- Blum, L. W., Q. Schiller, X. Li, R. Millan, A. Halford, and L. Woodger (2013), New conjunctive CubeSat and balloon measurements to quantify rapid energetic electron precipitation, *Geophys. Res. Lett.*, *40*, 5833–5837, doi:10.1002/2013GL058546.
- Blum, L. W., X. Li, and M. Denton (2015), Rapid MeV electron precipitation as observed by SAMPEX/HILT during high speed stream driven storms, *J. Geophys. Res. Space Physics*, *120*, 3783–3794, doi:10.1002/2014JA020633.
- Bortnik, J., R. M. Thorne, T. P. O'Brien, J. C. Green, R. J. Strangeway, Y. Y. Shprits, and D. N. Baker (2006), Observation of two distinct, rapid loss mechanisms during the 20 November 2003 radiation belt dropout event, *J. Geophys. Res.*, *111*, A12216, doi:10.1029/2006JA011802.
- Carson, B. R., C. J. Rodger, and M. A. Clilverd (2013), POES satellite observations of EMIC-wave driven relativistic electron precipitation during 1998–2010, *J. Geophys. Res. Space Physics*, *118*, 232–243, doi:10.1029/2012JA017998.
- Chen, L., J. Bortnik, R. M. Thorne, R. B. Horne, and V. K. Jordanova (2009), Three-dimensional ray tracing of VLF waves in a magnetospheric environment containing a plasmaspheric plume, *Geophys. Res. Lett.*, *36*, L22101, doi:10.1029/2009GL040451.
- Clilverd, M. A., R. Duthie, R. Hardman, A. T. Hendry, C. J. Rodger, T. Raita, M. Engebretson, M. R. Lessard, D. Danskin, and D. K. Milling (2015), Electron precipitation from EMIC waves: A case study from 31 May 2013, *J. Geophys. Res. Space Physics*, *120*, 3618–3631, doi:10.1002/2015JA021090.
- Comess, M. D., D. M. Smith, R. S. Selesnick, R. M. Millan, and J. G. Sample (2013), Duskside relativistic electron precipitation as measured by SAMPEX: A statistical survey, *J. Geophys. Res. Space Physics*, *118*, 5050–5058, doi:10.1002/jgra.50481.
- Cornwall, J. M., and M. Schulz (1971), Electromagnetic ion-cyclotron instabilities in multicomponent magnetospheric plasmas, *J. Geophys. Res.*, *76*(31), 7791–7796, doi:10.1029/JA076i031p07791.
- Cornwall, J. M., F. V. Coroniti, and R. M. Thorne (1970), Turbulent loss of ring current protons, *J. Geophys. Res.*, *75*(25), 4699–4709, doi:10.1029/JA075i025p04699.
- de Soria-Santacruz, M., M. Spasojevic, and L. Chen (2013), EMIC waves growth and guiding in the presence of cold plasma density irregularities, *Geophys. Res. Lett.*, *40*, 1940–1944, doi:10.1002/grl.50484.
- Denton, R. E., V. K. Jordanova, and B. J. Fraser (2014), Effect of spatial density variation and  $O^+$  concentration on the growth and evolution of electromagnetic ion cyclotron waves, *J. Geophys. Res. Space Physics*, *119*, 8372–8395, doi:10.1002/2014JA020384.
- Engebretson, M. J., et al. (2008), Pc1-Pc2 waves and energetic particle precipitation during and after magnetic storms: Superposed epoch analysis and case studies, *J. Geophys. Res.*, *113*, A01211, doi:10.1029/2007JA012362.
- Erlanson, R. E., and A. E. Ukhorskiy (2001), Observations of electromagnetic ion cyclotron waves during geomagnetic storms: Wave occurrence and pitch angle scattering, *J. Geophys. Res.*, *106*(A3), 3883–3895, doi:10.1029/2000JA000083.
- Foat, J. E., R. P. Lin, D. M. Smith, F. Fenrich, R. Millan, I. Roth, K. R. Lorentzen, M. P. McCarthy, G. K. Parks, and J. P. Treilhou (1998), First detection of a terrestrial MeV X-ray burst, *Geophys. Res. Lett.*, *25*, 4109–4112, doi:10.1029/1998GL900134.
- Gendrin, R. (1975), Is the plasmapause a preferential region for proton precipitation?, *Ann. Geophys.*, *31*, 127.
- Goldstein, J., S. D. Pascuale, C. Kletzing, W. Kurth, K. J. Genestreti, R. M. Skoug, B. A. Larsen, L. M. Kistler, C. Mouikis, and H. Spence (2014a), Simulation of Van Allen Probes plasmapause encounters, *J. Geophys. Res. Space Physics*, *119*, 7464–7484, doi:10.1002/2014JA020252.
- Goldstein, J., M. F. Thomsen, and A. DeJong (2014b), In situ signatures of residual plasmaspheric plumes: Observations and simulation, *J. Geophys. Res. Space Physics*, *119*, 4706–4722, doi:10.1002/2014JA019953.
- Halford, A. J., B. J. Fraser, and S. K. Morley (2010), EMIC wave activity during geomagnetic storm and nonstorm periods: CRRES results, *J. Geophys. Res.*, *115*, A12248, doi:10.1029/2010JA015716.
- Halford, A. J., B. J. Fraser, and S. K. Morley (2015), EMIC waves and plasmaspheric and plume density: CRRES results, *J. Geophys. Res. Space Physics*, *120*, 1974–1992, doi:10.1002/2014JA020338.
- Imhof, W. L., H. D. Voss, J. B. Reagan, D. W. Datlowe, E. E. Gaines, and J. Mobilia (1986), Relativistic electron and energetic ion precipitation spikes near the plasmapause, *J. Geophys. Res.*, *91*(A3), 3077–3088, doi:10.1029/JA091iA03p03077.
- Jordanova, V. K., Y. S. Miyoshi, S. Zaharia, M. F. Thomsen, G. D. Reeves, D. S. Evans, C. G. Mouikis, and J. F. Fennell (2006), Kinetic simulations of ring current evolution during the Geospace Environment Modeling challenge events, *J. Geophys. Res.*, *111*, A11510, doi:10.1029/2006JA011644.
- Jordanova, V. K., J. Albert, and Y. Miyoshi (2008), Relativistic electron precipitation by EMIC waves from self-consistent global simulations, *J. Geophys. Res.*, *113*, A00A10, doi:10.1029/2008JA013239.
- Keika, K., K. Takahashi, A. Y. Ukhorskiy, and Y. Miyoshi (2013), Global characteristics of electromagnetic ion cyclotron waves: Occurrence rate and its storm dependence, *J. Geophys. Res. Space Physics*, *118*, 4135–4150, doi:10.1002/jgra.50385.
- Li, X., et al. (2012), Colorado Student Space Weather Experiment: Differential flux measurements of energetic particles in a highly inclined low Earth orbit, in *Dynamics of the Earth's Radiation Belts and Inner Magnetosphere*, *Geophys. Monogr. Ser.*, vol. 199, edited by D. Summers et al., pp. 385–404, AGU, Washington, D. C., doi:10.1029/2012GM001313.
- Li, Z., et al. (2014), Investigation of EMIC wave scattering as the cause for the BARREL 17 January 2013 relativistic electron precipitation event: A quantitative comparison of simulation with observations, *Geophys. Res. Lett.*, *41*, 8722–8729, doi:10.1002/2014GL062273.
- Lorentzen, K. R., M. P. McCarthy, G. K. Parks, J. E. Foat, R. M. Millan, D. M. Smith, R. P. Lin, and J. P. Treilhou (2000), Precipitation of relativistic electrons by interaction with electromagnetic ion cyclotron waves, *J. Geophys. Res.*, *105*(A3), 5381–5389, doi:10.1029/1999JA000283.
- Lyons, L. R., and R. M. Thorne (1972), Parasitic pitch angle diffusion of radiation belt particles by ion cyclotron waves, *J. Geophys. Res.*, *77*, 5608–5616, doi:10.1029/JA077i028p05608.
- Mann, I. R., et al. (2008), The upgraded CARISMA magnetometer array in the THEMIS era, *Space Sci. Rev.*, *141*, 413–451, doi:10.1007/s11214-008-9457-6.
- McCollough, J. P., J. L. Gannon, D. N. Baker, and M. Gehmeyr (2008), A statistical comparison of commonly used external magnetic field models, *Space Weather*, *6*, S10001, doi:10.1029/2008SW000391.

- McCollough, J. P., S. R. Elkington, M. E. Usanova, I. R. Mann, D. N. Baker, and Z. C. Kale (2010), Physical mechanisms of compressional EMIC wave growth, *J. Geophys. Res.*, *115*, A10214, doi:10.1029/2010JA015393.
- Meredith, N. P., R. B. Horne, T. Kersten, B. J. Fraser, and R. S. Grew (2014), Global morphology and spectral properties of EMIC waves derived from CRRES observations, *J. Geophys. Res. Space Physics*, *119*, 5328–5342, doi:10.1002/2014JA020064.
- Millan, R. M., and R. M. Thorne (2007), Review of radiation belt relativistic electron losses, *J. Atmos. Sol. Terr. Phys.*, *69*, 362.
- Millan, R. M., R. P. Lin, D. M. Smith, K. R. Lorentzen, and M. P. McCarthy (2002), X-ray observations of MeV electron precipitation with a balloon-borne germanium spectrometer, *Geophys. Res. Lett.*, *29*(24), 2194, doi:10.1029/2002GL015922.
- Millan, R. M., et al. (2013), The Balloon Array for RBSP Relativistic Electron Losses (BARREL), *Space Sci. Rev.*, *179*, 503–530, doi:10.1007/s11214-013-9971-z.
- Min, K., J. Lee, K. Keika, and W. Li (2012), Global distribution of EMIC waves derived from THEMIS observations, *J. Geophys. Res.*, *117*, A05219, doi:10.1029/2012JA017515.
- Miyoshi, Y., K. Sakaguchi, K. Shiokawa, D. Evans, J. Albert, M. Connors, and V. Jordanova (2008), Precipitation of radiation belt electrons by EMIC waves, observed from ground and space, *Geophys. Res. Lett.*, *35*, L23101, doi:10.1029/2008GL035727.
- Nakamura, R., M. Isowa, Y. Kamide, D. N. Baker, J. B. Blake, and M. Looper (2000), SAMPEX observations of precipitation bursts in the outer radiation belt, *J. Geophys. Res.*, *105*(A7), 15,875–15,885, doi:10.1029/2000JA900018.
- Olson, J. V., and L. C. Lee (1983), Pc1 wave generation by sudden impulses, *Planet. Space Sci.*, *31*(3), 295–302, doi:10.1016/0032-0633(83)90079-X.
- Sandanger, M., F. Søråas, K. Aarsnes, K. Oksavik, and D. S. Evans (2007), Loss of relativistic electrons: Evidence for pitch angle scattering by electromagnetic ion cyclotron waves excited by unstable ring current protons, *J. Geophys. Res.*, *112*, A12213, doi:10.1029/2006JA012138.
- Singer, H. J., L. Matheson, R. Grubb, A. Newman and S. D. Bouwer (1996), Monitoring space weather with the GOES magnetometers, *SPIE Conference Proceedings, GOES-8 and Beyond*, vol. 2812, edited by E. R. Washwell, pp. 299–308.
- Summers, D., and R. M. Thorne (2003), Relativistic electron pitch-angle scattering by electromagnetic ion cyclotron waves during geomagnetic storms, *J. Geophys. Res.*, *108*(A4), 1143, doi:10.1029/2002JA009489.
- Thorne, R. M., and C. F. Kennel (1971), Relativistic electron precipitation during magnetic storm main phase, *J. Geophys. Res.*, *76*(19), 4446–4453, doi:10.1029/JA076i019p04446.
- Tsyganenko, N. A. (1989), A magnetospheric magnetic field model with a warped tail current sheet, *Planet. Space Sci.*, *37*, 5–20, doi:10.1016/0032-0633(89)90066-4.
- Ukhorskiy, A. Y., Y. Y. Shprits, B. J. Anderson, K. Takahashi, and R. M. Thorne (2010), Rapid scattering of radiation belt electrons by storm time EMIC waves, *Geophys. Res. Lett.*, *37*, L09101, doi:10.1029/2010GL042906.
- Usanova, M. E., I. R. Mann, J. Bortnik, L. Shao, and V. Angelopoulos (2012), THEMIS observations of electromagnetic ion cyclotron wave occurrence: Dependence on AE, SYMH, and solar wind dynamic pressure, *J. Geophys. Res.*, *117*, A10218, doi:10.1029/2012JA018049.
- Vampola, A. L. (1977), The effect of strong pitch angle scattering on the location of the outer-zone electron boundary as observed by low-altitude satellites, *J. Geophys. Res.*, *82*(16), 2289–2294, doi:10.1029/JA082i016p02289.
- Wang, Z., Z. Yuan, M. Li, H. Li, D. Wang, H. Li, S. Huang, and Z. Qiao (2014), Statistical characteristics of EMIC wave-driven relativistic electron precipitation with observations of POES satellites: Revisit, *J. Geophys. Res. Space Physics*, *119*, 5509–5519, doi:10.1002/2014JA020082.
- Woodger, L. A., A. J. Halford, R. M. Millan, M. P. McCarthy, D. M. Smith, G. S. Bowers, J. G. Sample, B. R. Anderson, and X. Liang (2015), A summary of the BARREL campaigns: Technique for studying electron precipitation, *J. Geophys. Res. Space Physics*, *120*, doi:10.1002/2014JA020874.